The impact of simultaneous intracranial recordings on scalp EEG: a finite element analysis

Simeon M Wong[1,2], Rohit Sharma[3], Ahmed Abushama[3], Ayako Ochi[3], Hiroshi Otsubo[3], George M Ibrahim[1,2,4,5]

1. Neurosciences and Mental Health, Hospital for Sick Children, Toronto, Canada
2. Institute of Biomedical Engineering, University of Toronto, Toronto, Canada
3. Department of Neurology, Hospital for Sick Children, Toronto, Canada
4. Division of Neurosurgery, Hospital for Sick Children, Toronto, Canada
5. Department of Surgery, University of Toronto, Toronto, Canada

Corresponding Author
Dr. George M Ibrahim
george.ibrahim@sickkids.ca

The Hospital for Sick Children
Division of Neurosurgery
555 University Avenue
Toronto Ontario M5G 1X8
Canada

Abstract

Background

In this study, we examined the utility of simultaneous scalp and stereotactic intracranial electroencephalography (SSIEEG) in epilepsy patients. Although SSIEEG offers valuable insights into epilepsy and cognitive function, its routine use is uncommon. Challenges include interpreting post-craniotomy scalp EEG due to surgically implanted electrodes.

New Method

We describe our methodology for conducting SSIEEG recordings. To simulate the potential impact on EEG interpretation, we computed the leadfield of scalp electrodes with and without burrholes using Finite Element Analysis to compare the resulting sensitivity volume and waveforms of simulated intracranial signals between skulls with and without burrholes.

Results

The presence of burr holes in the skull layer of the leadfield models did not discernibly modify simulated waveforms or scalp EEG topology. Using realistic SEEG burr hole diameter, the difference in the average leadfield of scalp electrodes was 0.12% relative to the effect of switching two nearby electrodes, characterized by the cosine similarity difference. No patients experienced adverse events related to SSIEEG.

Comparison with Existing Methods

Although there is increasing acceptance and interest in SSIEEG, few studies have characterized the technical feasibility. Here, we demonstrate through modelling that scalp recordings from SSIEEG are comparable to that through an intact skull.

Conclusion

The placement and simultaneous acquisition of scalp EEG during invasive monitoring through stereotactically inserted EEG electrodes is routinely performed at the Hospital for Sick Children. Scalp EEG recordings may assist with clinical interpretation. Burr holes in the skull layer did not discernibly alter EEG waveforms or topology.

Keywords
Intracranial electroencephalography; Scalp electroencephalography; Finite element analysis; Simulation; Burr holes; Leadfield

1. Introduction

In this short communication, we describe our experiences and observations while carrying out simultaneous scalp and stereotactic intracranial electroencephalography (SSIEEG) monitoring on pediatric patients under consideration for epilepsy surgery. While separate scalp EEG and stereoelectroencephalography (sEEG) recordings are routinely used individually in many clinical and research settings, the utility and interpretability of simultaneous recordings have been questioned.

A number of studies have described simultaneous intracranial and scalp recordings, focusing on the visibility and topology on scalp recordings of medial temporal spikes [1] and frontal lobe spikes [2], the sensitivity of scalp EEG for seizure detection [3,4], and even reports demonstrating source localization from a SSIEEG with a dense scalp array [5]. SSIEEG also unlocks a rich dataset for studying mechanisms and biomarkers of epilepsy [6] and cognitive function [7,8]. Despite the demonstrated utility, the routine use of SSIEEG for invasive monitoring in epilepsy centers remains relatively uncommon[9].

One notable challenge is the potential for difficulty in interpreting scalp EEG in the post-craniotomy period, due to changes in conductivity and other physiological alterations associated with the surgical procedure[10]. The effects of multiple small openings, as is performed with sEEG is poorly studied. Classically, disruptions in the skull bone were thought to cause the breach rhythm, but later studies suggest this was unlikely to arise from changes to electrical conductivity[11]. Bénar and colleagues[12] have previously modelled the effect of burr holes on EEG, but focused on impact to inverse modelling and dipole localization in relation to larger 10 mm burr holes.

We therefore present simulation results demonstrating the limited impact of sEEG burr holes on the topology and waveform of scalp EEG recordings, with a focus on the impact to scalp EEG topology and amplitude. Additionally, we describe our experience and insights at a large academic pediatric epilepsy center with the collection of simultaneous scalp and intracranial EEG data.

2. Methods

2.1. Electrode Application and Recordings

Consecutive case series. To enhance the yield of clinically relevant EEG data and exclude seizure propagation from regions not directly monitored by sEEG, we introduced the use of scalp EEG electrodes at the Hospital for Sick Children in Toronto, Canada in 2017. In this consecutive series of 31 sEEG cases, 26 received SSIEEG. Five intracranial sEEG patients did not receive scalp EEG because our institution initially only applied scalp EEG electrodes to patients where global patterns of epilepsy may be under-represented by the sEEG placement, and not to all patients receiving sEEG. Over time, scalp electrodes had become standard for all patients undergoing sEEG.

Electrodes. sEEG electrodes (0.86mm diameter, AdTech Medical) were inserted under general anesthesia following placement of 2.4 mm diameter burr holes. Trajectories are planned with Renishaw

software and guided by the Renishaw neuromate. MRI-safe and CT-compatible scalp electrodes (Rhythmlink International) were applied with collodion, using the international 10-20 system, with a minimum 10 mm distance from any SEEG bolt. Any required deviations from established locations are made symmetrically and documented on a head diagram. Between 12 to 19 electrodes are applied per patient, depending on clinical requirements. Impedance is kept below 10 Ohms. ECG, EMG, and SpO2 are also recorded simultaneously.

Recordings. The data from both the scalp and SEEG electrodes were recorded on a Natus Quantum amplifier (Natus Neurology), at 2048 Hz and 16-bit resolution. The EEG data obtained from SSIEEG are referential to a silent intracranial electrode, selected by a board-certified epileptologist.

Ethics. This retrospective study was approved by the Hospital for Sick Children Research Ethics Board.

2.2. Waveform and Electrical Propagation Simulations

Electrode localization. The post-insertion head Computed Tomography (CT) images from a representative sEEG case with a lateralized hypothesis were used to manually identify the locations of intracranial electrodes in subject space. This information was subsequently co-registered with pre-operative T1 Magnetic Resonance Imaging (MRI) scans employing FSL's linear image registration tool (FLIRT), then transformed into MNI space using FSL's non-linear image registration tool (FNIRT)[13]. These post-insertion trajectories were used to simulate burr holes in realistic locations.

Finite Element Modelling (FEM) setup. The 0.5 mm isometric ICBM 2009b nonlinear asymmetric adult template[14] was loaded into Fieldtrip[15] and segmented into scalp, skull, cerebrospinal fluid (CSF), and brain tissues. FEM models were constructed using Simbio[16] with hexahedral elements and default tissue conductivity values (1.79 S/m CSF; 0.33 S/m scalp; 0.01 S/m skull; 0.33 S/m brain). To model the impact of surgical procedures on the scalp, simulated burr holes were created based on the intracranial electrode localizations derived from the post-insertion CT images. Skull bone elements in contact with an imaginary cylinder within specified distance (eg. 2.5 mm) of the center of the insertion line were replaced with CSF model elements, and the FEM models were recomputed. The standard 10-20 electrode locations were then loaded from the Fieldtrip template.

Simulations were also run on the ICBM 10–14-year-old pediatric template[14] (see supplementary materials) with the adult template being the more conservative of the two. Therefore, the adult template was selected for its higher resolution, larger base dataset, and the similarity in skull anatomy between our youngest SEEG patient and the adult template[17].

FEM forward model & leadfield. Finally, forward leadfield models were computed for both the intact and perforated FEM models on a 5 mm isometric intracranial source grid. The leadfield represents the recorded electrical activity at an electrode given a unit electrical current at given locations in the brain, in this study, with locations placed on an isometric 5 mm grid throughout the brain tissue. The leadfield is derived from physical models of electrical propagation across tissues, which in this study, is the FEM model. In other words, the leadfield tells us "what the EEG electrode sees" given a defined electrical source within the brain.

Cosine similarity and vector norm. To evaluate differences in the leadfields computed for an intact skull and a skull with SEEG burr holes, we used the vector norm difference (VND) and the cosine similarity difference (CSD). The CSD is a measure of similarity between two vectors determined by the cosine of the angle between them, reflecting the spatial pattern similarity between leadfields. In this context, CSD can be considered as a measure of the relative difference in the composition of the recorded signal, while the VND indexes the relative alteration in signal amplitude (Figure 1A).

We note that high CSD (CSD→1) indicates similar spatial patterns, whereas low values (CSD→0) suggest dissimilarity. As the cosine similarity index measures orientation, it allows us to assess spatial patterns independent of magnitude. Thus, through the combined use of vector norm and cosine similarity, we are able to quantify both changes in signal magnitude and alterations in spatial patterns and morphology.

Simulated scalp recordings. We projected intracranially recorded epileptic electroencephalogram (EEG) waveforms and background EEG activity through intact and perforated leadfields at the standard 2.5 mm diameter to simulate the visual differences, if any, in propagation due to stereoelectroencephalography (SEEG) burr holes. This approach allowed us to visually confirm the potential impact of burr holes on subsequent EEG waveform simulations.

Code availability. The MATLAB and Python code used to run the simulations and generate the figures in this report are freely available at https://github.com/gmilab/SSIEEG_simulations.

3. Results

3.1. Simulations: effect of burr hole diameter

Using a FEM model, we simulated the effect of 10 burr holes for a typical insular hypothesis implantation at different burr hole diameters. To provide context for the numerical scale, the CSD and VND between the C3 and C4 electrodes and the Fz and Cz electrodes on an intact skull were also computed (Figure 1B).

With the standard 2.5 mm burr hole diameter, the mean (95% CI) CSD between an intact skull and a skull with burr holes was 6.30 (0.83-32.74) x 10^{-4}, or 0.08% of the CSD between C3 and C4 electrodes. The mean VND was 1.31 (0.33-4.28) x 10^{-4}, or 5% of the VND between C3 and C4 electrodes. At 20 mm, a diameter that is unrealistic in the context of SEEG, the mean CSD is 0.088 (0.011-0.401), translating to 11.3% of the CSD between C3 and C4. Burr holes appear to have a larger impact on scalp EEG amplitude than topology or the receptive field of each scalp electrode.

3.2. Simulations: effect of burr holes on leadfield topology

Using the FEM model with 10 burr holes of 2.5 mm, we show the scalp topology of the leadfield for the Left Mid Frontal, Left Superior Parietal, and the Left Mid Temporal gyri from the Automated Anatomical Labelling atlas[18]. The scalp topologies (Figure 1C) of the leadfield illustrate the amplitude recorded by

scalp electrodes, for a unit current at the centroid of each region. No remarkable topological differences are observed between intact and 2.5 mm burrhole models as the difference map shows largely similar topology with raw values. The amplitude between models is also small relative to the raw values with the maximum amplitude differences an order of magnitude lower.

Simulations: effect of burr hole diameter on scalp EEG amplitude

Using the FEM model with 10 burr holes, we show the root-mean-square (RMS) leadfield values for every scalp electrode compared between varying hole diameters to explore the effect of burr holes on scalp EEG amplitudes. In contrast with the above analyses, here we show the RMS values directly and not the difference between models. The RMS of the leadfield provides a direct estimate of RMS EEG amplitude[16]:$Y \approx L \times S$ where $Y = [y_1, y_2, \ldots y_n]$ and denotes the EEG recorded at the scalp at the i-th electrode, $L \in R^{m \times n}$ denotes the leadfield matrix, and $S = [s_1, \ldots, s_m]$ denotes the neural source activity within the brain. We observe that the difference between models with burr holes, even at larger sizes, is small relative to the RMS leadfield of the intact model.

3.3. Simulations: effect of burr hole distance

Using a FEM model with a single burr hole under Cz and surface electrodes placed anteriorly on the midline with 1mm spacing, we simulated the effect of distance between a recording electrode and the burr hole on CSD and VND (Figure 1E).

The maximum CSD and VND at any of the tested distances was 2.43 x 10^{-3} and 7.21 x 10^{-5}, respectively. Both CSD and VND are relatively high within 15 mm of the burrhole, with a minima in the CSD for a hypothetical electrode placed between 20 to 50 mm from the burr hole.

3.4. Simulations: effect of intracranial distance from burr hole

Using the FEM model with 10 burr holes, we placed intracranial sources spaced at 5 mm distances immediately beneath a burr hole, and projected a unit current at each source location through the models constructed with and without 2.5 mm burr holes to the simulated scalp EEG sensors. The resulting amplitude is shown topologically for both models, alongside the difference between models. Increasing source depth results in a lower amplitude, more diffuse topology (Figure 1F). The largest differences between models are observed in sources closest to the burr hole and to the surface, whereas the deeper sources with more diffuse topologies have relatively smaller differences between models.

3.5. Simulations: spike projection to scalp

In this example case with a left insular hypothesis, we simulated a left insula interictal epileptiform discharge as recorded on the scalp using both intact and perforated skull models. We observe no visually distinguishable difference between the two models (Figure 2A), as expected due to the small differences in their leadfields as shown earlier.

3.6. Clinical Utility in Representative Case

To illustrate the clinical utility of simultaneous scalp and SEEG, we present the case of a 15.5-year-old right-handed female patient with a 7-year history of seizures and a known diagnosis of Tuberous sclerosis complex 1 (TSC1).

Neuropsychological assessments were non-localizing and non-lateralizing. Pre-operative video EEG (vEEG), Magnetoencephalography (MEG), and clinical correlation suggested a seizure onset in the left temporal and insular regions, leading to a strong left-lateralized hypothesis and insertion of sEEG electrodes only in left hemisphere for frontal, temporal, and insular targets for seizure localization and language mapping.

Despite the strong left-lateralized hypothesis, a non-habitual seizure captured through the simultaneous scalp and SEEG procedure was found to originate from the right hemisphere, contradicting initial findings. Importantly, this seizure's ictal onset was observed 18 seconds earlier on the scalp EEG than on the SEEG channels (Figure 2B). This case illustrates the valuable clinical insights that can be gained from simultaneous scalp and SEEG. Without the inclusion of scalp EEG, the onset of this non-habitual seizure would not have been reliably localized.

3.7. Safety and Practicality of Simultaneous Scalp and Intracranial EEG

From 2017 to 2022, 31 pediatric patients were admitted to SickKids for invasive monitoring using stereotactic EEG (SEEG). Of these patients, 26 successfully received simultaneous scalp and SEEG, demonstrating the practicality of the procedure. Importantly, no additional cases of surgical site infection or adverse events were reported, highlighting the safety of the procedure. Application of the scalp EEG required an additional 45 minutes during headwrap application, a modest increase in procedure time.

3.8. Research Utility of Scalp EEG

The implementation of simultaneous scalp and SEEG opened new avenues for research. The scalp EEG has been utilized in pilot studies and for establishing baselines in computer-based neuropsychological tasks. Moreover, bedside scalp EEG provided a critical context and comparison to research task baselines, further demonstrating its research utility. We have now published several studies leveraging SSIEEG recordings[7,8,19,20].

4. Discussion

Our findings at the Hospital for Sick Children underline the potential benefits of routinely applying simultaneous scalp and stereo EEG in pediatric epilepsy patients undergoing invasive monitoring. We observed that the addition of scalp EEG did not exacerbate risk factors or adverse events, indicating that the combined approach maintains patient safety.

In our simulations with realistic scalp, skull, and brain models, we find that standard 2.5 mm burr holes have a negligible impact on the transmission of intracranial electrical currents to scalp electrodes as indexed by VND and CSD between the intact and burr hole leadfields (Figure 1b). These aggregate measures provide an overall view of change in the leadfield from all possible cranial generator sources directly analogous to the aggregate electrical potentials recorded by a scalp EEG electrode. Therefore, we also characterized the impact of individual cortical generators in a region of highest likely impact: directly inferior to a burr hole (Figure 1f). We observed nearly no change in topology and minimal change in amplitude, noting that the scale of the topomaps are 4 orders of magnitude smaller than those between neighboring scalp electrodes (cf. Figure 1a). Finally, we observe a negligible impact on the interpretability of the data corroborating our leadfield findings (Figure 2a).

Although the scalp EEG procedure necessitates a slight extension in headwrap application time, the incremental cost is outweighed by the valuable data acquired. The opportunity to record non-habitual seizures, demonstrated in our case study, highlights the importance of this additional information in enhancing seizure pattern understanding and improving preoperative evaluations.

5. Conclusions

Given the safety, practicality, and additional clinical insights provided, we recommend the routine application of simultaneous scalp and stereo EEG, particularly for the capture of potential non-habitual seizures. The integration of these techniques can augment research opportunities and optimize clinical decision-making. Further investigations are warranted to fully explore the potential of this approach in varied patient groups and clinical scenarios.

Competing interests

The authors declare no competing interests.

Author contributions

Simeon Wong: Conceptualization, methodology, software, investigation, analysis, validation, writing – draft, writing – review & editing, visualization; **Rohit Sharma**: Conceptualization, data curation, resources, , administration, writing – review & editing; **Ahmed Abushama**: analysis, investigation, data curation, writing – review & editing; **Ayako Ochi**: conceptualization, validation, resources, data curation, writing – review & editing; **Hiroshi Otsubo**: conceptualization, validation, resources, data curation, writing – review & editing; **George Ibrahim**: conceptualization, methodology, validation, investigation, resources, writing – review & editing, supervision.

6. Figures

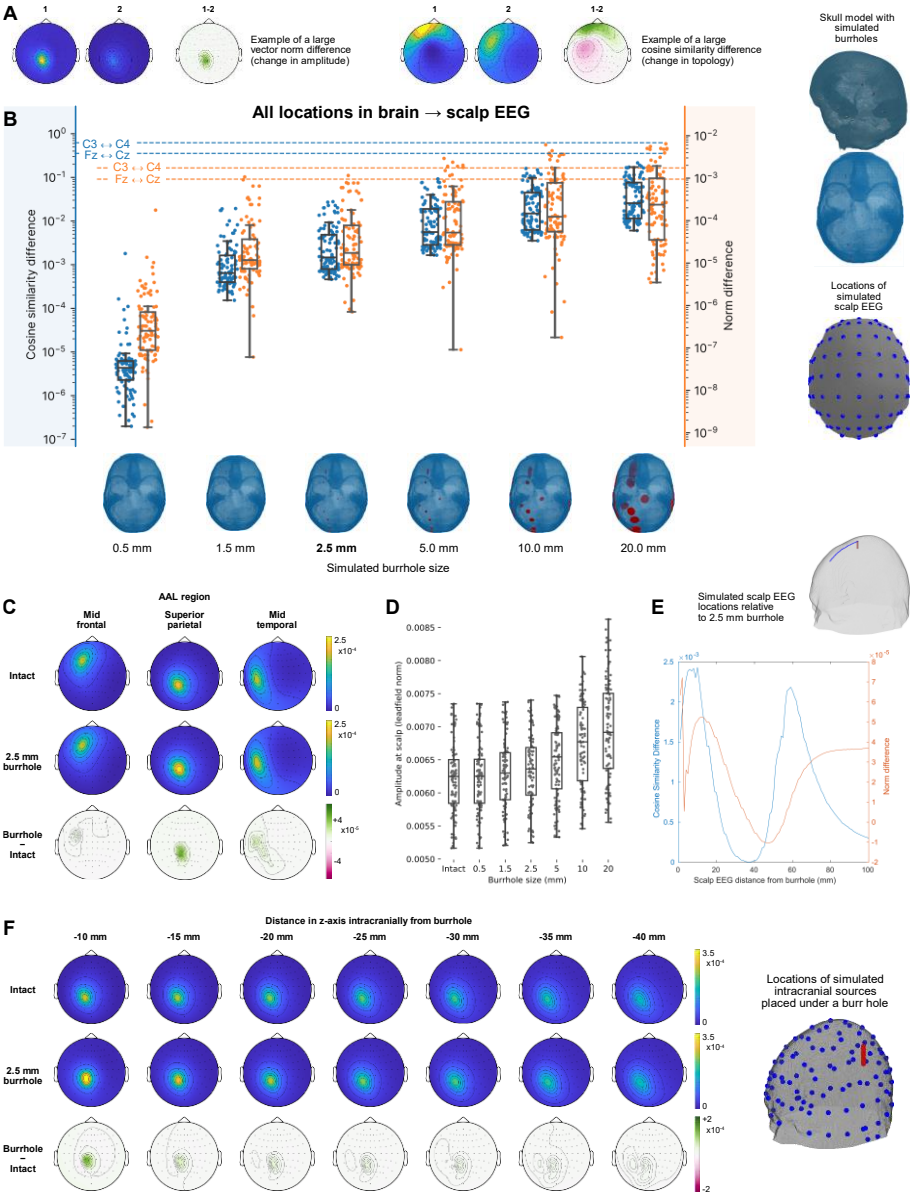

Figure 1. (A) Example topologies illustrating VND and CSD. (B) The CSD (blue) and VND (orange) between the intact model and the burr hole model are shown for increasing burr hole diameters. As a scale reference, the CSD and VND between swapped electrode pairs on an intact skull are shown with dotted lines. In the 3D render of the skull mesh, simulated burr holes indicated in red and the 10-20 electrode placements in the model are in blue. (C) Impact of 2.5 mm burr holes on scalp topology of intracranial sources at three representative AAL regions. (D) Effect of burr holes of increasing diameter on measured EEG amplitude, indexed by the leadfield norm. (E) In a model with a single burr hole under Cz, the CSD (blue) and VND (orange) are shown for a hypothetical electrode placed on the midline with increasing distance anteriorly to the burr hole. (F) Effect of 2.5 mm burr holes on the topology of a single intracranial EEG source with increasing source depth.

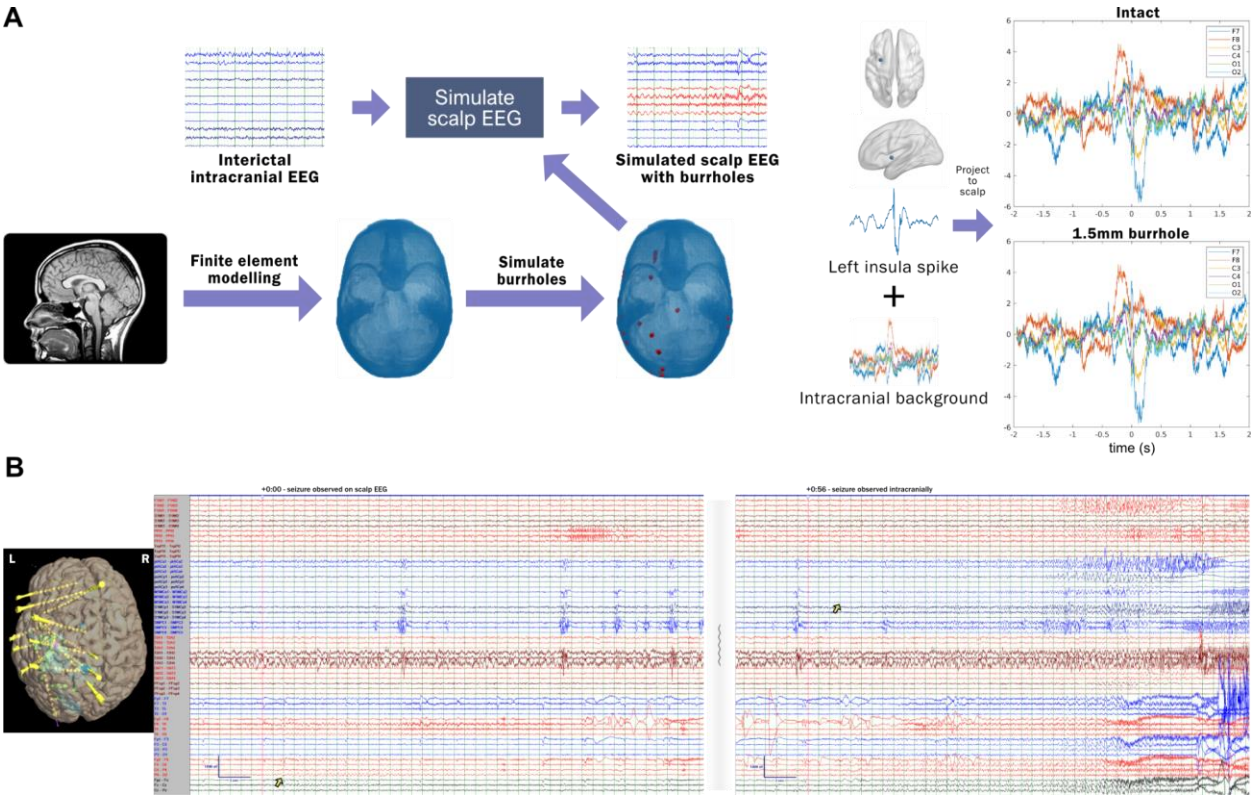

Figure 2. (A) Overview of our simulation pipeline and the resulting projection of a simulated insular spike to scalp sensors with and without intracranial background noise show no appreciable difference between intact skull and one with simulated burr holes. (B) Selected montage from the representative case demonstrating clinical utility of SSIEEG during the pre-ictal and early-ictal of a seizure originating contralateral to the hypothesized laterality for invasive monitoring. The first electrographic indication of seizure begins on the left panel as indicated, in a scalp channel. The earliest intracranial indication of seizure initiation is visible in the right panel 38 seconds later.

7. References

1. Koessler L, Cecchin T, Colnat-Coulbois S, et al. Catching the invisible: mesial temporal source contribution to simultaneous EEG and SEEG recordings. *Brain Topogr*. 2015;28(1):5-20. doi:10.1007/s10548-014-0417-z

2. Ramantani G, Dümpelmann M, Koessler L, et al. Simultaneous subdural and scalp EEG correlates of frontal lobe epileptic sources. *Epilepsia*. 2014;55(2):278-288. doi:10.1111/epi.12512

3. Casale MJ, Marcuse LV, Young JJ, et al. The Sensitivity of Scalp EEG at Detecting Seizures—A Simultaneous Scalp and Stereo EEG Study. *J Clin Neurophysiol*. 2022;39(1):78. doi:10.1097/WNP.0000000000000739

4. Yamazaki M, Tucker DM, Fujimoto A, et al. Comparison of dense array EEG with simultaneous intracranial EEG for interictal spike detection and localization. *Epilepsy Res*. 2012;98(2-3):166-173. doi:10.1016/j.eplepsyres.2011.09.007

5. Yamazaki M, Tucker DM, Terrill M, Fujimoto A, Yamamoto T. Dense array EEG source estimation in neocortical epilepsy. *Front Neurol*. 2013;4:42. doi:10.3389/fneur.2013.00042

6. De Stefano P, Carboni M, Marquis R, Spinelli L, Seeck M, Vulliemoz S. Increased delta power as a scalp marker of epileptic activity: a simultaneous scalp and intracranial electroencephalography study. *Eur J Neurol*. 2022;29(1):26-35. doi:10.1111/ene.15106

7. Wong SM, Arski ON, Warsi NM, et al. Phase Resetting in the Anterior Cingulate Cortex Subserves Childhood Attention and Is Impaired by Epilepsy. *Cereb Cortex*. 2021;32(1):29-40. doi:10.1093/cercor/bhab192

8. Arski ON, Wong SM, Warsi NM, et al. Epilepsy disrupts hippocampal phase precision and impairs working memory. *Epilepsia*. 2022;63(10):2583-2596. doi:10.1111/epi.17357

9. Antony AR, Abramovici S, Krafty RT, et al. Simultaneous scalp EEG improves seizure lateralization during unilateral intracranial EEG evaluation in temporal lobe epilepsy. *Seizure*. 2019;64:8-15. doi:10.1016/j.seizure.2018.11.015

10. Mader EC Jr, Miller D, Toler JM, Olejniczak PW. Focal Epileptiform Discharges Can Mimic Electrode Artifacts When Recorded on the Scalp Near a Skull Defect. *J Investig Med High Impact Case Rep*. 2018;6:2324709618795305. doi:10.1177/2324709618795305

11. Brigo F, Cicero R, Fiaschi A, Bongiovanni LG. The breach rhythm. *Clin Neurophysiol*. 2011;122(11):2116-2120. doi:10.1016/j.clinph.2011.07.024

12. Bénar CG, Gotman J. Modeling of post-surgical brain and skull defects in the EEG inverse problem with the boundary element method. *Clin Neurophysiol*. 2002;113(1):48-56. doi:10.1016/s1388-2457(01)00714-3

13. Jenkinson M, Beckmann CF, Behrens TEJ, Woolrich MW, Smith SM. FSL. *Neuroimage*. 2012;62(2):782-790. doi:10.1016/j.neuroimage.2011.09.015

14. Fonov V, Evans AC, Botteron K, et al. Unbiased average age-appropriate atlases for pediatric studies. *Neuroimage*. 2011;54(1):313-327. doi:10.1016/j.neuroimage.2010.07.033

15. Oostenveld R, Fries P, Maris E, Schoffelen JMM. FieldTrip: Open Source Software for Advanced Analysis of MEG, EEG, and Invasive Electrophysiological Data. *Comput Intell Neurosci*. 2011;2011:156869. doi:10.1155/2011/156869

16. Drechsler F, Wolters CH, Dierkes T, Si H, Grasedyck L. A full subtraction approach for finite element method based source analysis using constrained Delaunay tetrahedralisation. *Neuroimage*. 2009;46(4):1055-1065. doi:10.1016/j.neuroimage.2009.02.024

17. Farkas LG, Posnick JC, Hreczko TM. Anthropometric growth study of the head. *Cleft Palate Craniofac J*. 1992;29(4):303-308. doi:10.1597/1545-1569_1992_029_0303_agsoth_2.3.co_2

18. Tzourio-Mazoyer N, Landeau B, Papathanassiou D, et al. Automated Anatomical Labeling of Activations in SPM Using a Macroscopic Anatomical Parcellation of the MNI MRI Single-Subject Brain. *Neuroimage*. 2002;15(1):273-289. doi:10.1006/nimg.2001.0978

19. Warsi NM, Wong SM, Gorodetsky C, et al. Which is more deleterious to cognitive performance? Interictal epileptiform discharges vs anti-seizure medication. *Epilepsia*. 2023;64(5):e75-e81. doi:10.1111/epi.17556

20. Warsi NM, Wong SM, Suresh H, et al. Interictal discharges delay target-directed eye movements and impair attentional set-shifting in children with epilepsy. *Epilepsia*. 2022;63(10):2571-2582. doi:10.1111/epi.17365